JCI The Journal of Clinical Investigation

Impaired complex I repair causes recessive Leber's hereditary optic neuropathy

Sarah L. Stenton, … , Ilka Wittig, Holger Prokisch

J Clin Invest. 2021. https://doi.org/10.1172/JCI138267.

Research In-Press Preview Genetics Neuroscience

Graphical abstract

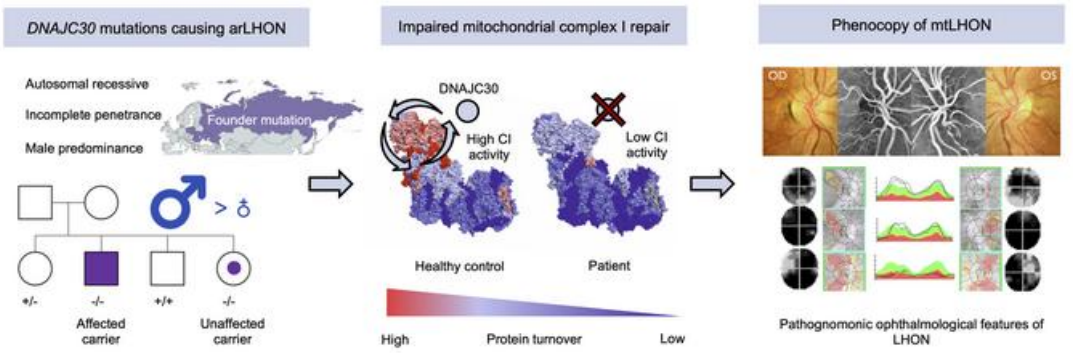

Title

Impaired complex I repair causes recessive Leber's hereditary optic neuropathy

Authors

Sarah L Stenton[1,2], Natalia L Sheremet[3], Claudia B Catarino[4], Natalia A Andreeva[3], Zahra Assouline[5], Piero Barboni[6], Ortal Barel[7,8,9], Riccardo Berutti[1,2], Igor Bychkov[10], Leonardo Caporali[11], Mariantonietta Capristo[11], Michele Carbonelli[11], Maria L Cascavilla[6], Peter Charbel Issa[12,13], Peter Freisinger[14], Sylvie Gerber[15], Daniele Ghezzi[16,17], Elisabeth Graf[1,2], Juliana Heidler[18], Maja Hempel[19], Elise Heon[20], Yulya S Itkis[10], Elisheva Javasky[7,8,9], Josseline Kaplan[15], Robert Kopajtich[1,2], Cornelia Kornblum[21], Reka Kovacs-Nagy[1,22], Tatiana D Krylova[10], Wolfram S Kunz[23], Chiara La Morgia[11,24], Costanza Lamperti[16], Christina Ludwig[25], Pedro F Malacarne[26], Alessandra Maresca[11], Johannes A Mayr[27], Jana Meisterknecht[18], Tatiana A Nevinitsyna[3], Flavia Palombo[11], Ben Pode-Shakked[8,28,29], Maria S Shmelkova[3], Tim M Strom[1], Francesca Tagliavini[11], Michal Tzadok[8,30], Amelie T van der Ven[19], Catherine Vignal-Clermont[31], Matias Wagner[1,2], Ekaterina Y Zakharova[10], Nino V Zhorzholadze[3], Jean-Michel Rozet[15], Valerio Carelli[11,24], Polina G Tsygankova[10], Thomas Klopstock[4,32,33], Ilka Wittig[18,34*], Holger Prokisch[1,2,*]

Affiliations

1. Institute of Human Genetics, School of Medicine, Technische Universität München, München, Germany.
2. Institute of Neurogenomics, Helmholtz Zentrum München, München, Germany.

3. Federal State Budgetary Institution of Science “Research Institute of Eye Diseases”, Moscow, Russia.
4. Department of Neurology, Friedrich-Baur-Institute, University Hospital of the Ludwig-Maximilians-Universität München, Munich, Germany.
5. Fédération de Génétique et Institut Imagine, Université Paris Descartes, Hôpital Necker Enfants Malades, Paris, France.
6. Scientific Institute San Raffaele, Milan, Italy.
7. Genomics Unit, Sheba Cancer Research Center, Sheba Medical Center, Tel-Hashomer, Israel.
8. Sackler Faculty of Medicine, Tel-Aviv University, Tel-Aviv, Israel.
9. Wohl Institute for Translational Medicine, Sheba Medical Center, Tel-Hashomer, Israel.
10. Research Centre for Medical Genetics, Moscow, Russia.
11. IRCCS Istituto delle Scienze Neurologiche di Bologna, Bologna, Italy.
12. Oxford Eye Hospital, Oxford University Hospitals NHS Foundation Trust, Oxford, UK.
13. Nuffield Laboratory of Ophthalmology, Department of Clinical Neurosciences, University of Oxford, Oxford, UK.
14. Department of Pediatrics, Klinikum am Steinenberg, Reutlingen, Germany.
15. Laboratory genetics in ophthalmology (LGO), INSERM UMR1163 - Institute of genetic diseases, Imagine. Paris, France.
16. Unit of Medical Genetics and Neurogenetics, Fondazione IRCCS Istituto Neurologico Carlo Besta, Milan, Italy.
17. Department of Pathophysiology and Transplantation, University of Milan, Italy.
18. Functional Proteomics, Medical School, Goethe University, Frankfurt am Main, Germany.
19. Institute of Human Genetics, University Medical Center Hamburg-Eppendorf, Hamburg, Germany.

20. The Hospital for Sick Children, Department of Ophthalmology and Vision Sciences, The University of Toronto, Toronto, Canada.
21. Department of Neurology, University Hospital Bonn, Bonn, Germany.
22. Department of Medical Chemistry, Molecular Biology and Pathobiochemistry, Semmelweis University, Budapest, Hungary.
23. Department of Experimental Epileptology and Cognition Research, University of Bonn, Bonn, Germany.
24. Unit of Neurology, Department of Biomedical and NeuroMotor Sciences (DIBINEM), University of Bologna, Italy.
25. Bavarian Center for Biomolecular Mass Spectrometry (BayBioMS), Technische Universität München, München, Germany.
26. Institute for Cardiovascular Physiology, Goethe-University, Frankfurt, Frankfurt am Main, Germany.
27. Department of Pediatrics, Salzburger Landeskliniken and Paracelsus Medical University Salzburg, Austria.
28. Institute for Rare Diseases, Edmond and Lily Safra Children's Hospital, Sheba Medical Center, Tel-Hashomer, Israel.
29. Talpiot Medical Leadership Program, Sheba Medical Center, Tel-Hashomer, Israel.
30. Pediatric Neurology Unit, Edmond and Lily Safra Children's Hospital, Sheba Medical.
31. Ophthalmology Department, Centre National d'Ophtalmologie des Qinze-Vingts, Paris, France.
32. German Center for Neurodegenerative Diseases (DZNE), Munich, Germany.
33. Munich Cluster of Systems Neurology (SyNergy), Munich, Germany.
34. German Center for Cardiovascular Research (DZHK), Partner site RheinMain, Frankfurt, Germany.

Corresponding authors

Dr. Ilka Wittig

Functional Proteomics, Goethe-Universität,

Frankfurt am Main, Germany

Email: wittig@med.uni-frankfurt.de

Number: +49 69 6301 4180

Dr. Holger Prokisch

Institut für Humangenetik, Klinikum rechts der Isar, Technische Universität München

Trogerstraße 32, 81675 München, Germany

E-mail: prokisch@helmholtz-muenchen.de

Number: +49 89 3187 2890

Conflict of interest statement

C.B.C., C.K., P.B., C.L.M., T.K., and V.C. have received research support, speaker honoraria, consulting fees, and travel costs from Santhera Pharmaceuticals and GenSight Biologics.

Complete word count

8,700

Abstract

Leber's hereditary optic neuropathy (LHON) is the most frequent mitochondrial disease and was the first to be genetically defined by a point mutation in the mitochondrial DNA (mtDNA). A molecular diagnosis is reached in up to 95%, the vast majority of which are accounted for by three mutations within mitochondrial complex I (CI) subunit encoding genes in the mtDNA (mtLHON). Here, we resolve the enigma of LHON in the absence of pathogenic mtDNA mutations. We describe biallelic mutations in a nuclear encoded gene, *DNAJC30*, in 33 unsolved patients from 29 families and establish an autosomal recessive mode of inheritance for LHON (arLHON), which to date has been a prime example of a maternally inherited disorder. Remarkably, all hallmarks of mtLHON are recapitulated, including incomplete penetrance, male predominance, and significant idebenone responsivity. Moreover, by tracking protein turnover in patient-derived cell lines and a *DNAJC30*-knock-out cellular model, we measure reduced turnover of specific CI N-module subunits and a resultant impairment of CI function. This demonstrates DNAJC30 is to be a chaperone protein needed for the efficient exchange of CI subunits exposed to reactive oxygen species and integral to a mitochondrial CI repair mechanism, thereby providing the first example of a disease resulting from impaired exchange of assembled respiratory chain subunits.

Introduction

Leber's hereditary optic neuropathy (LHON, OMIM:535000) was first noted by Von Graefe in 1858 (1) and was formally described as a clinical entity bearing his name by Leber in 1871 (2). LHON results from a rapidly evolving degenerative process and is thereby unique amongst the hereditary optic atrophies in its clinical course. It presents with subacute, simultaneous or

sequential, bilateral painless loss of central vision due to selective degeneration of the retinal ganglion cells (RGCs) and their axons. The disease arises during young adult life and displays a gender dependent incomplete penetrance of 50% in males and 10% in females (3), resulting in five times more males being affected. Permanent severe loss of central vision is the typical endpoint, though spontaneous recovery of visual acuity has occasionally been reported (4,5,6).

Though noted in its earliest descriptions to be transmitted through the maternal line (7), the inheritance pattern of LHON was only confirmed over one century later by the discovery of the first point mutation in the mitochondrial DNA (mtDNA) (m.11778G>A in *MT-ND4*) (8). Along with two further point mutations (m.3460G>A in *MT-ND1* and m.14484T>C in *MT-ND6*), all together these three mtDNA mutations account for approximately 90% of LHON cases with a maternal family history (3,9,10). Other rare mtDNA mutations account approximately for a further 5% (11), inclusive of variants associated with MELAS (Mitochondrial myopathy, encephalopathy, lactic acidosis, and stroke-like episodes, OMIM:540000) (12,13,14) and Leigh syndrome (infantile subacute necrotizing encephalopathy, OMIM:256000) (15,16).

LHON mutations characteristically disrupt subunits of mitochondrial complex I (CI), the first and largest of the electron transfer complexes, encoded by both the nuclear and mtDNA. CI is carefully assembled by numerous factors and associates with the other proton translocating complexes to form supercomplexes in the mitochondrial inner membrane. These complexes couple electron flow with proton pumping to generate the membrane potential which drives ATP synthesis (17,18,19). To maintain high functionality, CI subunits exposed to the highest levels of oxidative damage may undergo repair largely independent of the remaining complex,

by disassembly and replacement of subunits at a much lower energetic cost than *de novo* synthesis of the complex in its entirety (20,21).

Results

Identification of pathogenic *DNAJC30* mutations in LHON patients in association with a complex I defect

A homozygous missense variant in *DNAJC30* was initially identified by WES in four individuals from the German Network for Mitochondrial Disorders (mitoNET), three males from two families with adult-onset LHON and a female with childhood-onset Leigh syndrome. Through international collaboration within the European Network for Mitochondrial Disorders (GENOMIT), the combined analysis of WES data and Sanger sequencing of further molecularly undiagnosed LHON patients, revealed an additional 29 cases associated with *DNAJC30* mutations. mtDNA screening failed to detect any other pathogenic variants or rare variants of uncertain significance (VUS) (**Table S1**). Moreover, in those investigated by WES, no biallelic pathogenic variants or VUS were detected in nuclear genes encoding CI subunits or assembly factors (**Table S2**).

Of the 33 subjects, 29 harbored the same NM_032317.2 c.152A>G (7:73097602, NP_115693.2 p.Tyr51Cys) homozygous variant with an allele frequency of 0.125% (351:281136 alleles, no homozygous carriers) in gnomAD. The remaining four patients, from Family 18 and Family 20, harbored a NM_032317.2 c.232C>T (7:73097522, NP_115693.2, p.Pro78Ser) and a NM_032317.2 c.302T>A (7:73097452, NP_115693.2, p.Leu101Gln) homozygous variant, respectively, both of which are absent in gnomAD (**Figure 1A**).

Due to the recessive mode of inheritance, and therefore the absence of a family history, identification of pedigrees with unaffected homozygous carriers is challenging. Despite this, our collection of pedigrees indicates incomplete penetrance, with five homozygous mutation carriers not expressing a phenotype. In total, 30 of 31 (96.8%) homozygous carrier males and just three of seven (42.9%) homozygous carrier females express a phenotype. This results in a significant male predominance, with a 10:1 ratio of affected males to affected females ($p<0.001$, Fisher's exact test) (**Figure 1B**). The penetrance of the *DNAJC30* variants can only be approximated, and is unquestionably an overestimate due to the limited number of large pedigrees and unaffected siblings of differing carrier status in our study. Nevertheless, these observations resemble the incomplete penetrance associated with mtLHON, where penetrance is reported to be approximately 50% in males and 10% in females. This results in a 5:1 ratio of affected males to affected females (3,22) (**Figure 1B**). To investigate the underlying reason for the higher penetrance in males, we measured DNAJC30 expression on the RNA and protein level in over 75 and 100 controls, respectively, however failing to find a significant difference (**Figure S1A-B**). DNAJC30 availability is therefore not the factor influencing gender-dependent variable penetrance. In mtLHON, the mtDNA population-specific polymorphisms of haplogroup J are proposed play a modifying role in penetrance, as patients with the haplogroup J genetic background demonstrate higher penetrance (23). This association is recapitulated in arLHON, as 5 of 27 investigated arLHON patients (18.5%) have the haplogroup J genetic background, which is over the expected 9% for the European population (24) (**Table 1**).

Given that the majority of the patients originate from Russia, Poland, Romania, and Ukraine, the p.Tyr51Cys *DNAJC30* variant is ascribed to an Eastern European founder event. The

variant is estimated to have arisen 85 generations ago (confidence interval 43-168 generations) based on the genetic length of ancestral haplotypes shared between individuals (**Figure S1C**). Taking the allele frequency of the variant (0.125%) and applying the Hardy-Weinberg Equation with adjustment for the observed incomplete penetrance, arLHON is estimated to affect 1.09 per million individuals, a figure just below the established prevalence estimate of LHON once adjusted for the prior assumption that up to 95% are accounted for by mtDNA mutations (1.61 per million, 95% CI 1.24-1.99 per million) (25). Furthermore, in Russia, the contribution of *DNAJC30* variants to the heritability of LHON is considerably higher. Of 86 molecularly confirmed LHON patients investigated by full mtDNA sequencing and WES in the Research Centre for Medical Genetics in Moscow, 18 (20.9%) harbored the homozygous p.Tyr51Cys *DNAJC30* mutation, while 68 (79.1%) harbored pathogenic mtDNA mutations. Male prominence was demonstrated in both forms of LHON (arLHON 17:1 affected male to affected female ratio, mtLHON 15:2 affected male to affected female ratio). Additional evidence for incomplete penetrance is provided by screening of the Research Centre for Medical Genetics institutional database of WES data from 1036 patients with inherited disease, where we find 10 heterozygous carriers of the p.Tyr51Cys variant, indicating a MAF of 0.48% in the founder population. This predicts 2.3 per 100,000 homozygous carriers. If the variant were fully penetrant, this figure would exceed the expected number of LHON cases, thereby strengthening the argument for incomplete penetrance. The marked incomplete penetrance in females, is supported by an equal allele frequency in male and female individuals of the p.Tyr51Cys founder variant in the gnomAD database (male 0.12%, females 0.13%).

All three *DNAJC30* variants occur in a conserved area of the protein, the J domain (**Figure S1D**). This domain belongs to a family of chaperone proteins and is key to their functional interactions (26). The p.Tyr51Cys and p.Leu101Gln variants are positioned in close proximity

on the protein structure (**Figure S1E**) and lead to degradation of the protein (**Figure S1F**). These amino acids are therefore likely to be fundamental to the structural integrity of the protein. While, the p.Pro78Ser variant, which does not lead to protein degradation (**Figure S1F**), is predicted to disrupt function due to its position in a crucial functional region, the His, Pro, and Asp tripeptide (HPD) (26) (**Figure S1D**).

Consistent with mtLHON, a CI defect is invariably demonstrated on skeletal muscle biopsy in investigated arLHON patients (**Figure S1G**). CIV and CV activity is not disrupted (**Figure S1H-I**). Analyzing CI dependent respiration in patient-derived fibroblast cell lines (n=7) reveals a significant defect (mean 69% of control, s.d. 16%, $p<0.001$), which is modest yet consistent across patients and genotypes and is in keeping with, if not more subtle than, the magnitude of CI defect seen in mtDNA LHON patient-derived fibroblast cell lines (n=3) (**Figure S1J-K**). The CI dependent defect in respiration is rescued by re-expression of naïve-*DNAJC30* in the patient cell line (**Figure 1C**). Moreover, the CI dependent respiration defect is recapitulated in the *DNAJC30*-KO HEK cell line (mean 66% of control, s.d. 18%, $p<0.0001$) (**Figure 1C**).

LHON associated with *DNAJC30* mutations presents as a phenocopy of maternally inherited LHON

From a clinical perspective, physicians representing national centers of expertise in LHON were unable to stratify the LHON patients by mtDNA or nuclear origin. The pathognomonic triad of ophthalmological features: i) circumpapillary telangiectatic microangiopathy, ii) vessel tortuosity of the central retinal vessels without leakage on fluorescein angiography, and iii) the hallmark, subacute phase swelling (pseudoedema) of the retinal nerve fiber layer (RNFL) (27),

were documented in all arLHON subjects (**Table 2** and exemplified in **Figure 2A**). In all arLHON subjects the subacute phase was followed by an atrophic chronic phase with generalized thinning of the RNFL due to RGC and axonal degeneration. No macular or peripheral retinal abnormalities were reported, and brain magnetic resonance imaging (MRI) was reportedly normal in 19 of 22 investigated arLHON patients. There was no record of extra-ocular manifestations. In this regard, the clinical phenotype of arLHON is an indistinguishable phenocopy of mtLHON (see **Supplemental Methods** for individual patient case reports).

The statistical analysis uncovered subtle difference both in the age of onset and recovery rate of visual acuity in arLHON in comparison to mtLHON. The age of onset (mean 19.9 ± 7.9 years s.d.) is earlier and more condensed than reported for mtLHON (mean 30.7 ± 15.0 years s.d., $p<0.001$) (28) (**Table 1** and **Figure 2B**). Age-related expression of DNAJC30 on the RNA and protein level measured in control fibroblast cell lines was unable to provide an explanation for this pattern of onset (**Figure S2A-B**). The median time from involvement of the first eye to involvement of the second eye was one week (range 0 to 2 years) and 14 patients (46.7%) demonstrated bilateral involvement at onset. The median time from onset to nadir was eight weeks (range 0 to 2 years) (**Table 2**). We acknowledge that the natural history of the cohort may be confounded to some extent by the concurrent use of idebenone in the majority of the cases.

Clinically relevant recovery of visual impairment from nadir (CRR), defined as improvement in logMAR (Logarithm of the Minimum Angle of Resolution) visual acuity (VA) of ≥0.2 (29), was observed in 42 eyes (67.7%, in 22 patients). In eight eyes (12.9%, in six patients) VA recovery was complete (**Table 2**). Idebenone therapy was received by 18 patients, as a potent antioxidant and electron donor approved for LHON by EMA

(https://www.ema.europa.eu/en/medicines/human/EPAR/raxone) bypassing CI to restore downstream mitochondrial electron flow and respiration (29). Of the 36 treated and 26 untreated eyes, CRR was reported in 29 (80.6%) and 13 (50.0%), respectively. The treated recovery is significantly higher than reported for mtLHON (4,5,6) ($p<0.001$, Fisher's exact test) (**Figure 2C**). The mean time from onset to first CRR was 13.0 months ± s.d. 10.4 months, and 25.8 months ± s.d. 30.3 months, in the treated and untreated eyes, respectively. This is comparable to mtLHON where the mean time from onset to first CRR is reported to be 17.2 months ± s.d. 7.8 months in idebenone-treated cases, and 27.7 months ± s.d. 22.5 months in idebenone-naïve cases (5).

We also report one patient with Leigh syndrome in the absence of optic involvement. This is a female patient, presenting at two years of age with spasticity, dysarthria, disturbance of gait, a moderate lactate peak on magnetic resonance spectroscopy (MRS), and bilateral necrosis of the putamen with lesions in the pedunculi cerebelli suggestive of Leigh syndrome on brain MRI (see **Supplemental Methods** for the case report).

DNAJC30 mutations result in impaired exchange of specific subunits of mitochondrial complex I

Due to the consistent CI defect on the patient muscle biopsies, we analyzed quantitative proteomic data from patient-derived (n=3) and control (n=105) fibroblast cell lines, to determine whether DNAJC30 defects lead to a decrease in CI abundance. However, to our surprise, differential expression analysis (DEA) followed by gene set enrichment analysis for 149 mitochondrial pathways (MitoPathways3.0), demonstrated a subtle yet significant increase of 12.1% in "Complex I subunits" in the patient cell lines (adjusted p 0.04, based on mean

log2fc) (**Figure S3A, Table S3-S4**). Given the impaired CI dependent respiration in patient-derived fibroblast cell lines, this subtle increase in CI abundance results in low relative specific activity of CI ($p<0.0001$) (**Figure S3B**). There was no significant signal for any other OXPHOS complex to indicate a general increase in mitochondrial biogenesis (**Figure S3A, Table S3-S4**). The specificity of the DNAJC30 defect for CI was also confirmed by a subtle yet significant increase in CI in a quantitative proteomic analysis of DDM solubilised respiratory chain complexes (RCC) separated by blue native electrophoresis (BNE) in the *DNAJC30*-KO HEK cell line (p 0.0002) (**Figure S3C**). The abundance of the remaining respiratory chain complexes was not significantly increased (CIII p 0.38, CIV p 0.50).

To determine whether CI was properly assembled, we investigated a patient-derived fibroblast cell line and the *DNAJC30*-KO HEK cell line by complexome profiling. Here, we found intact and correctly assembled CI with no assembly intermediates in association with defective DNAJC30 (**Figure S3D-E**). Together with the quantitative proteomic data, these data confirmed that DNAJC30 is not a subunit or assembly factor of CI, which would be expected to decrease the abundance and disrupt the assembly of the complex. The complexome data also recapitulate loss of the DNAJC30 protein due to the p.Tyr51Cys founder mutation, as demonstrated in our earlier quantitative proteomic approach (**Figure S1F** and **S3D**), and confirmed the successful knock-out of DNAJC30 in the *DNAJC30*-KO HEK cell line (**Figure S3E**). Moreover, in the complexome profiling of the control fibroblast and control HEK cell lines, DNAJC30 was found to run at the size of the CI containing supercomplex, where it is present in substochiometric quantities (1:200 DNAJC30:CI), indicating a transient interaction with the CI containing supercomplex (**Figure S3D-E** and **Table S5**). The association of DNAJC30 with the CI containing supercomplex was supported across six independent quantitative proteomic experiments of digitonin solubilised RCC separated by BNE in our

study and by multiple previously published complexome datasets across human and mouse samples, as summarised in **Table S6**.

While the quantitative proteomic data in patient-derived fibroblast cell lines indicates a subtle increase in CI subunit abundance due to DNAJC30 defect, RNA sequencing did not reveal a corresponding increase in CI subunit expression, analyzed by a DEA of 149 mitochondrial pathways (MitoPathways3.0) between patient-derived fibroblast (n=3) and control fibroblast (n=79) cell lines (count data, **Table S7**, complete DEA results, **Table S8-9**). This indicated that there may be a problem in the degradation of CI subunits. We therefore measured the turnover of single proteins within mitochondrial protein complexes by combining pulse stable isotope labeling of amino acids in cell culture (pSILAC) with mass spectrometry of assembled RCC separated by BNE (see **Methods**).

It is known from recent studies that subunits of the CI N-module (**Figure 3A**) (30) require exchange, due to exposure to higher levels of oxidative damage (20-21). This results in higher turnover rates of the N-module subunits independent of the rest of the assembled complex. In the analysis of control fibroblast cell lines (n=7), we confirmed the presence of differential rates of turnover in the individual subunits of CI (**Figure 3B, Table S10-S15**). Moreover, we can further subdivide the CI subunits into three categories according to their respective turnover rates, as CI^{HIGH} and CI^{MOD} - together accounting for the N-module of CI - and CI^{LOW}, representing the remainder of CI. The CI^{HIGH} subunits (NDUFV3, NDUFS4, NDUFS6, NDUFA6, and NDUFA7) demonstrate a mean turnover of >25% in 12-hours in control fibroblasts cell lines (mean 33.6% ± 11.2% s.d.), while the CI^{LOW} subunits - accounting for the CI Q, ND1, ND2, ND4, and ND5-module subunits - have a mean turnover of 8.7% (± 6.0% s.d.). Each of these CI^{HIGH} subunits has been identified as a late participant in CI assembly according to Guerrero-Castillo et al., (31) indicating that these proteins are less stably bound

within the complex and might readily be exchangeable. The CI^{MOD} subunits, accounting for the remainder of the CI N-module subunits, have a mean turnover of 18.3% (± 5.7% s.d.).

The patient-derived fibroblast cell lines (n=6), spanning all three *DNAJC30* mutations, demonstrated a significant decrease in the turnover of N-module subunits in assembled CI (**Figure 3B** and **Table S10-S15**). The mean turnover of the CI^{HIGH} subunits is most strongly reduced to 16.8% from 33.6% ($p<0.0001$) followed by the CI^{MOD} subunits to 12.5% from 18.3% ($p<0.001$) (**Figure 3B-E, Table S10-S15**). In explanation of this finding, consultation of the Bioplex database of protein-protein interactions confirms four out of the five CI^{HIGH} proteins to be the direct interaction partners of DNAJC30, across five independent experiments (**Figure 3C**, complete results in **Table S16**) (32-33). Together, these data indicate that the interaction of DNAJC30 with specific CI subunits facilitates the high turnover of CI N-module subunits in a CI repair mechanism. This defect was not found in mtLHON (n=3) and is therefore specific to arLHON (**Figure 3D-E**). The defect shows no predilection to gender to account for the difference in gender dependent penetrance (**Figure S3F-G**).

To further validate these findings, and to question the specificity of the defect to CI, we studied the protein turnover of more than 1,200 proteins in the control and *DNAJC30*-KO HEK cell line, detecting 56 proteins with high turnover, defined as >25% at 12-hours. The data recapitulate the defect seen in the patient-derived fibroblast cell lines, with a mean turnover in CI^{HIGH} subunits of 31.0% in the *DNAJC30*-KO, in comparison to 48.7% in the control (p 0.013) (**Figure 3D**). This was also seen in the CI^{MOD} subunits, with a mean turnover of 24.5% in the *DNAJC30*-KO, in comparison to 36.6%. in the control (p 0.002) (**Figure 3E** and **Table S17**). In contrast, there is no DNAJC30-specific difference in the turnover of other CI subunits, all other OXPHOS subunits (including those with high turnover), and all other detected proteins with high turnover (**Figure S3H**). Moreover, by the analysis of differential protein turnover

within protein complexes (see **Supplemental Methods**), we verify that amongst all captured protein complexes (n=145), only mitochondrial CI, and specifically the CI N-module, had significantly altered turnover due to the knock-out of *DNAJC30* (mean delta turnover, 14.3% ± 7.6% s.d., adjusted p 0.04) (**Table S18**). Interestingly, among the top six mitochondrial proteins of similar phylogenetic profile to DNAJC30 are CLPX, CLPB, and the mitochondrial HSP70 (HSPA9), components of the mitochondrial protein degradation machinery (**Table S19**) (34).

We thereby propose DNAJC30 to be a chaperone protein involved in the exchange of CI^{HIGH} subunits (NDUFV3, NDUFS4, NDUFS6, NDUFA6, and NDUFA7), facilitating the protein degradation machinery, CLPXP, to access and degrade the N-module subunits exposed to higher levels of oxidative damage, and collectively maintaining CI with high function (**Figure 4A**). This functional link between DNAJC30 and CLPXP is supported by the evolutionary co-occurrence of both proteins. In contrast, in the absence of DNAJC30 the CI N-module subunits may no longer be readily exchangeable, resulting in an accumulation of CI with lower function, which is also reported in defects of the CLPXP subunits (20-21) (**Figure 4B**).

Discussion

Here we describe a recessive phenocopy of mtLHON due to mutations in the nuclear gene *DNAJC30*; where we observe incomplete penetrance and male predominance, phenomena seldom occurring in recessive disease. The evidence supporting these observations derives from the high allele frequency of the founder mutation and the equal distribution of the allele amongst genders in gnomAD, which should otherwise result in a common disease of equal gender distribution in the setting of full penetrance. Our data therefore indicate that the factor(s)

driving incomplete penetrance and male predominance originate downstream of the primary genetic event, secondary to subtle anatomical, hormonal, or otherwise physiological discrepancies between genders, or due to other genetic or epigenetic factors. Given that all investigated patient WES datasets were negative for rare biallelic variants in genes encoding CI subunits and assembly factors, and for rare mtDNA variants, we could not attribute the incomplete penetrance to a modifying factor at play in these genomic regions. Therefore, akin to mtLHON, the factor influencing gender dependent penetrance remains elusive at this time. Cautious interpretation of penetrance is required, both due to the relatively limited number of families on which to draw conclusions, and due to reports of the LHON phenotype manifesting up to the eighth decade of life (35). However, given that the vast majority of patients with arLHON express the disease in the second to third decade of life, and that the current age of almost all asymptomatic homozygous variant carriers is within the range of 30-50 years, it is expected that they will continue to be asymptomatic. A future epidemiological study would be necessitated to extensively explore this matter.

We provide molecularly undefined LHON patients with a diagnosis and demonstrate a further example of Leigh syndrome within a LHON/MELAS/Leigh syndrome spectrum. This also occasionally arises in specific rare mtDNA mutations affecting mtDNA encoded subunits of CI (15,16). In contrast to the infrequently described nuclear DNA abnormalities with "LHON-like" visual loss, such as in patients with Charcot-Marie-Tooth disease, in optic atrophy associated with dominant mutations in *OPA1* (36), and in a single report of recessive "LHON-like" optic neuropathy due to mutations in *NDUFS2* (37), our findings argue for the frequent occurrence of arLHON. This is effectively exemplified at the Research Centre for Medical Genetics in Moscow, where the p.Tyr51Cys *DNAJC30* founder mutation accounts for over 20% of molecularly diagnosed LHON patients. We therefore recommend parallel sequencing

of the complete mtDNA sequence and the one exon gene *DNAJC30* to close the diagnostic gap in LHON. Moreover, as arLHON is associated with an alternative mode of inheritance, an earlier age of onset, and a marked benefit from treatment with idebenone, even somewhat better than patients with mtLHON, reaching a genetic diagnosis has valuable implications in prognostic counselling and treatment decisions.

In arLHON, the mitochondrial CI defect characteristic of the disease results from the impaired exchange of specific CI N-module subunits exposed to higher risk of oxidative damage. The exchange of these subunits occurs at a lower energetic cost to complete *de novo* replacement of the complex and maintains high functionality (20,21,38,39). The subtlety of the CI dependent respiration defect in the patient-derived fibroblast cells lines reflects the role of DNAJC30 in maintenance rather than in the structure or assembly of CI; akin to a factor optimizing CI to ensure full bioenergetic function. The interaction of DNAJC30 with CI ascribes the protein to an additional function to that suggested to date, where DNAJC30 has been shown to play a role in mitochondrial and neuronal function and morphology by interaction with the ATP-synthase machinery (CV) to facilitate ATP synthesis (40). Complementary to our study of defective DNAJC30 in patient-derived fibroblast cell lines and in the *DNAJC30*-KO HEK cellular model, Tebbenkamp and colleagues demonstrated increased CI containing supercomplexes and hypofunctional mitochondria with significantly reduced respiration rate in cultured primary neurons from a *Dnajc30*-KO mouse model. Our data, however, did not demonstrate defective DNAJC30 to affect CV function in the patient muscle biopsies, CV abundance on proteomic analyses, nor CV subunit turnover. Clinically, defects in DNAJC30 have previously been suggested to contribute to the pathogenesis of William's syndrome, a 7q11.23 hemi-deletion of 26-28 genes inclusive of *DNAJC30*, which akin to LHON includes diminished neuronal function (40). However, both homozygous and

heterozygous *DNAJC30* variant carriers in our study displayed no clinical features of William's syndrome. Moreover, gnomAD reports 25 heterozygous loss-of-function variant carriers in addition to 351 heterozygous p.Tyr51Cys variant carriers which is also confirmed in our study to result in loss of the protein, comparable to a hemizygous deletion, in a reportedly healthy population. This argues that defects in DNAJC30, though potentially enhancing the phenotype of the haploinsufficiency of the genes within the William's syndrome locus, is alone unable to recapitulate all elements of phenotype.

To conclude, we resolve the enigma of the LHON phenotype in the absence of any pathogenic mtDNA mutations, and describe biallelic mutations of a nuclear encoded gene, *DNAJC30*, in so far unsolved LHON patients. This argues for "LHON" as a clinical description independent of transmission. Given this, we would suggest LHON to be subdivided as mtLHON and arLHON, due to the important impact on genetic counselling. With a combination of incomplete penetrance and higher than expected allele frequency, the discovery of this disease gene proved challenging to current diagnostic approaches. Moreover, we unveil the pathomechanism of recessive LHON and gain insight in a biological pathway. We demonstrate DNAJC30 to be a chaperone protein integral to a CI repair mechanism, controlling the exchange of CI subunits likely damaged by exposure to reactive oxygen species. As dysfunctional CI is the most frequent biochemical feature of mitochondrial disease (41,42) and is broadly implicated in the pathogenesis of cancer, diabetes, parkinsonism, and aging (43, 44,45), this study highlights DNAJC30 as a target within the CI repair pathway with potential therapeutic implications far beyond the optic neuropathies.

Methods

Study subjects. Clinical diagnosis of LHON was established by experienced ophthalmologists and neurologists specialized in mitochondrial disease across institutions in Germany, Italy, United Kingdom, France, Russia, Canada, and Israel. The clinical features of each patient are presented in **Table 1** and **Table 2**. Detailed case reports are presented in the **Supplemental Methods**.

Cell Lines and Tissue Culture. Patient-derived fibroblast cell lines were obtained by skin biopsy from the responsible clinician with written informed consent. NHDF (Normal Human Dermal Fibroblasts) were obtained from Lonza. HEK293 cells were obtained from Thermo Fisher Scientific. All cell lines were grown in Dulbecco's Modified Eagle Medium (DMEM, Life Technologies), supplemented with 10% fetal bovine serum (FBS), 1% penicillin/streptomycin, and 200 μM uridine. The culture medium was replaced once every 2-3 days. Cell lines were grown at 37°C in the presence of 5% CO_2. All patient-derived fibroblast cell lines were tested negative for mycoplasma contamination. Selective growth of the *DNAJC30* transfected cell line was maintained by the supplementation of blasticidin 5 μg/ml to the cell culture medium. Selective growth of *DNAJC30*-KO HEK cell line was maintained by the supplementation of puromycin 0.5 μg/ml to the cell culture medium.

Generation of the *DNAJC30* HEK293 knock-out cell line. The commercially available Origene KN2.0 non-homology mediated CRISPR knockout kit was utilized according to the manufacturer's instructions. Biallelic knock-out of *DNAJC30* resulted from donor integration on the first allele and a c.158_159insA (NM_032317.2) frameshift mutation on second allele

leading to premature stop codon within the J domain (p.Leu53Leufs*58, NP_115693.2) and complete loss of the protein on proteomic analyses.

Blue native electrophoresis. Sample preparation and blue native electrophoresis (BNE) of cultured cell pellets were essentially done as described in (46). Briefly, cells were collected by scraping and centrifugation, further disrupted using a pre-cooled motor-driven glass/Teflon Potter-Elvehjem homogenizer at 2000 rpm and 40 strokes. Homogenates were centrifuged for 15 min at 600 g to remove nuclei, cell debris, and intact cells. Mitochondrial membranes were sedimented by centrifugation of the supernatant for 15 min at 22,000g. Mitochondria enriched membranes from 20 mg cells were resuspended in 35 µl solubilization buffer (50 mM imidazole pH 7, 50 mM NaCl, 1 mM EDTA, 2 mM aminocaproic acid) and solubilized with 10 µl 20% digitonin (Serva) or 5µl 20% dodecylmaltoside. Samples were supplemented with 2.5 µl 5% Coomassie G250 in 500 mM aminocaproic acid and 5 µl 0.1% Ponceau S in 50% glycerol. Equal protein amounts of samples were loaded on top of a 3 to 18% acrylamide gradient gel (dimension 14x14 cm). After native electrophoresis in a cold chamber, blue-native gels were fixed in 50% (v/v) methanol, 10% (v/v) acetic acid, 10 mM ammonium acetate for 30 min and stained with Coomassie (0.025% Serva Blue G, 10% (v/v) acetic acid).

Mass spectrometry of assembled RCC separated by blue native electrophoresis (BNE). Procedures and parameters for mass spectrometry and data analysis were summarized at PRIDE-proteomics identification database with the identifiers PXD021385, PXD021386, PXD021500, PXD022340, PXD022339 and PXD021548.

pSILAC metabolic labeling. For pSILAC metabolic labeling, medium was changed into medium containing $^{13}C_6$,$^{15}N_4$-L-Arginine and $^{13}C_6$,$^{15}N_2$-L-Lysine (Silantes) for 0, 6, 8, 10 and

12 hours. Mitochondrial membranes were solubilized with either digitonin (Patient run 1, 2, 4, and HEK run, as per **Table S10**) or DDM (detergent dodecyl maltoside, Patient run 3, as per **Table S10**), protein complexes separated by BNE and the band(s) representing either the supercomplex and CV or the individual complexes, in digitonin and DDM solubilization respectively, were used for mass spectrometry. For protein turnover the ratio of heavy intensity-based absolute quantification (IBAQ) / sum of light and heavy IBAQ was calculated. Pymol version 2.3.3 was used to generate turnover heatmap in mouse CI structure (PDB 6g2) (30).

Statistical analysis. All statistical analyses were performed with R version 1.1.423. The choice of statistical test was determined by visual inspection of the distribution of the data. Where assumptions of normality and equal variance were met, the parametric two-sided Student's t-test was used to compare the means of two groups. When multiple comparisons were made to a control, the p values were corrected with the Dunnett's test. Categorical data were analyzed by the Fisher's exact test. The statistical test is stated in the respective figure legend. All reported p values are two-tailed with Bonferroni correction for multiple testing. A $p \leq 0.05$ was considered statistically significant. The p values are annotated in the figures by: $p \leq 0.05$ (*), $p \leq 0.01$ (**), $p \leq 0.001$ (***), and $p \leq 0.0001$ (****).

Additional information. Whole exome sequencing (WES) was performed as described in (37,47,48). RNA sequencing was performed as described in (47). Complementation of patient-derived fibroblast cell lines was performed by lentivirus-mediated expression of the full-length *DNAJC30* cDNA using the ViraPower HiPerform Lentiviral TOPO Expression Kit (Thermo Fisher Scientific) according to (49). Measurement of oxygen consumption rate (CI dependent

respiration rate) was performed as described by (49). All other methods and data analyses appear in the **Supplemental Methods**.

Study approval. This study was in accordance with the ethical principles of the Declaration of Helsinki and received local ethical committee approval from each center for their respective patient(s). Written informed consent was obtained from all patients, parents, or legal guardians as required.

Data availability. The proteomics data are available in ProteomeXchange via the PRIDE (50) partner repository with the identifiers: PXD021385, PXD021386, PXD021500, PXD022340, PXD022339, PXD021548, and PXD021499.

Author contributions

Conceived and designed study, H.P.; wrote the manuscript, S.L.S and H.P.; edited manuscript, all authors; performed experiments, S.L.S., T.D.K., W.S.K., C.L., and I.W.; analyzed results, S.L.S. and I.W.; provided essential materials, C.B.C., N.A.A., A.Z., P.B., O.B., I.B., L.C., M.C., M.C., M.L.C., P.C.I., P.F., S.G., D.G., J.H., M.H., E.H., Y.S.I., E.J., K.J., R.K., C.K., R.N.K., T.D.K., W.S.K., C.L.M., C.L., C.L., P.F.M., A.M., J.A.M., J.M., T.A.N., F.P., B.P., M.S.S., T.M.S., F.T., M.T., A.T.V., C.V., M.W., E.Y.Z., N.V.Z., J.M.R., V.C., P.G.T., T.K.; wrote the manuscript, S.L.S.; provided funding and supervision, H.P., I.W., T.K., D.G., C.L. and V.C.

Acknowledgements

This study was supported by a German Federal Ministry of Education and Research (BMBF, Bonn, Germany) grant to the German Network for Mitochondrial Disorders (mitoNET, 01GM1906D to I.W., H.P. and 01GM1906A to T.K.), by the German BMBF and Horizon2020 through the E-Rare project GENOMIT (01GM1920A to H.P., T.K., J.M., C.L.) and the ERA PerMed project PerMiM (01KU2016A to H.P. and D.G.), by the Italian Ministry of Health (GR-2016-02361449 to L.C. and by the "Ricerca Corrente" funding to V.C.), by the Deutsche Forschungsgemeinschaft (DFG) (SFB 815/Z1 to I.W.), and by the Cardio Pulmonary Institute (CPI) of the DFG (EXC2026 and TRR267-Z02 to I.W.). We would also like to thank Dr. Maria Lucia Valentino, Dr. Lidia Di Vito and Prof. Rocco Liguori from the IRCCS Istituto delle Scienze Neurologiche di Bologna, Bellaria Hospital and Department of biomedical and neuromotor Sciences, University of Bologna, Bologna, Italy for their contribution of a clinical neurological assessment and muscle histology investigation of one family, to thank Dr. Iris Ben-Bassat, Prof. Annick Raas-Rothschild, Prof. Raz Somech, Prof. Yair Anikster, and Prof. Bruria Ben-Zeev from the Sheba Medical Center, Tel-Hashomer, Israel, for their contribution of the clinical assessment of two families, and to thank Dr. Maria Logacheva from the Lomonosov Moscow State University for performing sequencing analyses.

References

1. Von Graefe, A. Exceptionelles verrhalten des gesichtsfeldes bei pigmentenartung der netzhaut. *Von Graefe's Arch Ophtlalmol*. 1858;4:250-253.
2. Leber, T. H. Ueber hereditäre und congenital-angelegte Sehnervenleiden. *Albrecht von Graefes Archiv für Ophthalmologie*. 1871;17(2):249-291.

3. Yu-Wai-Man, P., Votruba, M., Burté, F., La Morgia, C., Barboni, P., & Carelli, V. A neurodegenerative perspective on mitochondrial optic neuropathies. *Acta neuropathologica*. 2016;132(6):789-806.
4. Catarino, C. B., von Livonius, B., Priglinger, C., Banik, R., Matloob, S., Tamhankar, M. A., ... & Traber, G. L. Real-World Clinical Experience With Idebenone in the Treatment of Leber Hereditary Optic Neuropathy. *Journal of Neuro-Ophthalmology*. 2020;40(4):558.
5. Carelli, V., La Morgia, C., Valentino, M. L., Rizzo, G., Carbonelli, M., De Negri, A. M., ... & Sadun, A. A. Idebenone treatment in Leber's hereditary optic neuropathy. *Brain*. 2011;134(9): e188-e188.
6. Mashima, Y., Kigasawa, K., Wakakura, M., & Oguchi, Y. Do idebenone and vitamin therapy shorten the time to achieve visual recovery in Leber hereditary optic neuropathy?. *Journal of Neuro Ophthalmology*. 2000;20(3):166-170.
7. Erickson, R. P. Leber's optic atrophy, a possible example of maternal inheritance. *American journal of human genetics.* 1972;24(3):348.
8. Wallace, D. C., Singh, G., Lott, M. T., Hodge, J. A., Schurr, T. G., Lezza, A. M., ... & Nikoskelainen, E. K. Mitochondrial DNA mutation associated with Leber's hereditary optic neuropathy. *Science*. 1988;242(4884):1427-1430.
9. Howell, N., Bindoff, L. A., McCullough, D. A., Kubacka, I., Poulton, J., Mackey, D., ... & Turnbull, D. M. Leber hereditary optic neuropathy: identification of the same mitochondrial ND1 mutation in six pedigrees. *American journal of human genetics.* 1991;49(5):939.
10. Mackey, D. A., Oostra, R. J., Rosenberg, T., Nikoskelainen, E., Bronte-Stewart, J., Poulton, J., ... & Norby, S. Primary pathogenic mtDNA mutations in multigeneration pedigrees with Leber hereditary optic neuropathy. *American journal of human genetics.* 1996;59(2):481.

11. Achilli, A., Iommarini, L., Olivieri, A., Pala, M., Kashani, B. H., Reynier, P., ... & Barboni, P. Rare primary mitochondrial DNA mutations and probable synergistic variants in Leber's hereditary optic neuropathy. *PLoS One.* 2012;7(8).
12. Blakely, E. L., de Silva, R., King, A., Schwarzer, V., Harrower, T., Dawidek, G., ... & Taylor, R. W. LHON/MELAS overlap syndrome associated with a mitochondrial MTND1 gene mutation. *European Journal of Human Genetics*. 2005;13(5):623-627.
13. Pulkes, T., Eunson, L., Patterson, V., Siddiqui, A., Wood, N. W., Nelson, I. P., ... & Hanna, M. G. The mitochondrial DNA G13513A transition in ND5 is associated with a LHON/MELAS overlap syndrome and may be a frequent cause of MELAS. *Annals of neurology*. 1999;46(6):916-919.
14. Spruijt, L., Smeets, H. J., Hendrickx, A., Bettink-Remeijer, M. W., Maat-Kievit, A., Schoonderwoerd, K. C., ... & Hintzen, R. Q. A MELAS-associated ND1 mutation causing leber hereditary optic neuropathy and spastic dystonia. *Archives of neurology.* 2007;64(6):890-893.
15. Fruhman, G., Landsverk, M. L., Lotze, T. E., Hunter, J. V., Wangler, M. F., Adesina, A. M., ... & Scaglia, F. Atypical presentation of Leigh syndrome associated with a Leber hereditary optic neuropathy primary mitochondrial DNA mutation. *Molecular genetics and metabolism.* 2011;103(2):153-160.
16. Miyaue, N., Yamanishi, Y., Tada, S., Ando, R., Yabe, H., Nagai, M., & Nomoto, M. Repetitive brainstem lesions in mitochondrial DNA 11778G> A mutation of Leber hereditary optic neuropathy. *eNeurologicalSci*. 2019;14:74.
17. Brandt, U. Energy converting NADH: quinone oxidoreductase (complex I). *Annu. Rev. Biochem.* 2006;75:69-92.
18. Hirst, J. Mitochondrial complex I. *Annual review of biochemistry*. 2013;82:551-575.
19. Milenkovic, D., Blaza, J. N., Larsson, N. G., & Hirst, J. The enigma of the respiratory chain supercomplex. *Cell metabolism*. 2017;25(4):765-776.

20. Szczepanowska, K., Senft, K., Heidler, J., Herholz, M., Kukat, A., Höhne, M. N., ... & Zwicker, K. A salvage pathway maintains highly functional respiratory complex I. *Nature communications.* 2020;11(1):1-18.

21. Bogenhagen, D. F., & Haley, J. D. Pulse-chase SILAC–based analyses reveal selective oversynthesis and rapid turnover of mitochondrial protein components of respiratory complexes. *Journal of Biological Chemistry.* 2020;295(9):2544-2554.

22. Nikoskelainen, E. K., Huoponen, K., Juvonen, V., Lamminen, T., Nummelin, K., & Savontaus, M. L. Ophthalmologic findings in Leber hereditary optic neuropathy, with special reference to mtDNA mutations. *Ophthalmology.* 1996;103(3):504-514.

23. Hudson, G., Carelli, V., Spruijt, L., Gerards, M., Mowbray, C., Achilli, A., Pyle, A., Elson, J., Howell, N., La Morgia, C. and Valentino, M.L. Clinical expression of Leber hereditary optic neuropathy is affected by the mitochondrial DNA–haplogroup background. *The American Journal of Human Genetics.* 2007;81(2):228-233.

24. Pala, M., Olivieri, A., Achilli, A., Accetturo, M., Metspalu, E., Reidla, M., ... & Perego, U. A. Mitochondrial DNA signals of late glacial recolonization of Europe from near eastern refugia. *The American journal of human genetics.* 2012;90(5):915-924.

25. Man, P. Y. W., Griffiths, P. G., Brown, D. T., Howell, N., Turnbull, D. M., & Chinnery, P. F. The epidemiology of Leber hereditary optic neuropathy in the North East of England. *The American Journal of Human Genetics*. 2003;72(2):333-339.

26. Kampinga, H. H., & Craig, E. A. The HSP70 chaperone machinery: J proteins as drivers of functional specificity. *Nature reviews Molecular cell biology.* 2010;11(8):579-592.

27. Carelli, V., Ross-Cisneros, F. N., & Sadun, A. A. *Mitochondrial dysfunction as a cause of optic neuropathies. Progress in retinal and eye research.* 2005;23(1):53-89.

28. Rosenberg, T., Nørby, S., Schwartz, M., Saillard, J., Magalhaes, P. J., Leroy, D., ... & Duno, M. Prevalence and genetics of Leber hereditary optic neuropathy in the Danish population. *Investigative ophthalmology & visual science*. 2016;57(3):1370-1375.

29. Klopstock, T., Yu-Wai-Man, P., Dimitriadis, K., Rouleau, J., Heck, S., Bailie, M., ... & Kernt, M. A randomized placebo-controlled trial of idebenone in Leber's hereditary optic neuropathy. *Brain.* 2011;134(9):2677-2686.

30. Agip, A. N. A., Blaza, J. N., Bridges, H. R., Viscomi, C., Rawson, S., Muench, S. P., & Hirst, J. Cryo-EM structures of complex I from mouse heart mitochondria in two biochemically defined states. *Nature structural & molecular biology.* 2018;25(7):548-556.

31. Guerrero-Castillo, S., Baertling, F., Kownatzki, D., Wessels, H. J., Arnold, S., Brandt, U., & Nijtmans, L. The assembly pathway of mitochondrial respiratory chain complex I. *Cell metabolism*. 2017;25(1):128-139.

32. Huttlin, E. L., Bruckner, R. J., Paulo, J. A., Cannon, J. R., Ting, L., Baltier, K., ... & Szpyt, J. Architecture of the human interactome defines protein communities and disease networks. *Nature.* 2017;545(7655):505-509.

33. Huttlin, E. L., Ting, L., Bruckner, R. J., Gebreab, F., Gygi, M. P., Szpyt, J., ... & Dong, R. The BioPlex network: a systematic exploration of the human interactome. *Cell.* 2015;162(2):425-440.

34. Cheng, Y., & Perocchi, F. ProtPhylo: identification of protein–phenotype and protein–protein functional associations via phylogenetic profiling. *Nucleic acids research*. 2015;43(W1):W160-W168.

35. Dimitriadis, K., Leonhardt, M., Yu-Wai-Man, P., Kirkman, M. A., Korsten, A., De Coo, I. F., ... & Klopstock, T. Leber's hereditary optic neuropathy with late disease onset: clinical and molecular characteristics of 20 patients. *Orphanet journal of rare diseases.* 2014;9(1):158.

36. Yu-Wai-Man, P., Griffiths, P. G., & Chinnery, P. F. Mitochondrial optic neuropathies–disease mechanisms and therapeutic strategies. *Progress in retinal and eye research.* 2011;30(2):81-114.

37. Gerber, S., Ding, M. G., Gérard, X., Zwicker, K., Zanlonghi, X., Rio, M., ... & Bianchi, L. Compound heterozygosity for severe and hypomorphic NDUFS2 mutations cause non-syndromic LHON-like optic neuropathy. *Journal of medical genetics*. 2017;54(5):346-356.

38. Dröse, S., & Brandt, U. Molecular mechanisms of superoxide production by the mitochondrial respiratory chain. In Mitochondrial oxidative phosphorylation. *Springer, New York, NY.* 2012:145-169

39. Hirst, J., & Roessler, M. M. Energy conversion, redox catalysis and generation of reactive oxygen species by respiratory complex I. *Biochimica et Biophysica Acta (BBA)-Bioenergetics.* 2016;1857(7):872-883.

40. Tebbenkamp, A. T., Varela, L., Choi, J., Paredes, M. I., Giani, A. M., Song, J. E., ... & Li, M. The 7q11. 23 protein DNAJC30 interacts with ATP synthase and links mitochondria to brain development. *Cell.* 2018;175(4):1088-1104.

41. Distelmaier, F., Koopman, W. J., van den Heuvel, L. P., Rodenburg, R. J., Mayatepek, E., Willems, P. H., & Smeitink, J. A. Mitochondrial complex I deficiency: from organelle dysfunction to clinical disease. *Brain.* 2009;132(4):833-842.

42. Janssen, R. J., Nijtmans, L. G., Heuvel, L. P. V. D., & Smeitink, J. A. Mitochondrial complex I: structure, function and pathology. *Journal of Inherited Metabolic Disease: Official Journal of the Society for the Study of Inborn Errors of Metabolism*. 2006;29(4):499-515.

43. Fiedorczuk, K., & Sazanov, L. A. Mammalian mitochondrial complex I structure and disease-causing mutations. *Trends in cell biology.* 2018;28(10):835-867.

44. Urra, F. A., Muñoz, F., Lovy, A., & Cárdenas, C. The mitochondrial complex (I) ty of cancer. *Frontiers in oncology.* 2017;7:118.

45. Stefanatos, R., & Sanz, A. Mitochondrial complex I: a central regulator of the aging process. *Cell Cycle.* 2011;10(10):1528-1532.

46. Wittig, I., Braun, H. P., & Schägger, H. Blue native PAGE. *Nature protocols*. 2006;1(1):418.

47. Kremer, L. S., Bader, D. M., Mertes, C., Kopajtich, R., Pichler, G., Iuso, A., ... & Koňaříková, E. Genetic diagnosis of Mendelian disorders via RNA sequencing. *Nature communications.* 2017;8(1):1-11.

48. Del Dotto, V., Ullah, F., Di Meo, I., Magini, P., Gusic, M., Maresca, A., ... & Macao, B. SSBP1 mutations cause mtDNA depletion underlying a complex optic atrophy disorder. *The Journal of clinical investigation.* 2009;130(1):108-125.

49. Kremer, L. S., & Prokisch, H. Identification of disease-causing mutations by functional complementation of patient-derived fibroblast cell lines. In Mitochondria. *Humana Press, New York, NY.* 2017: 391-406.

50. Perez-Riverol, Y., Csordas, A., Bai, J., Bernal-Llinares, M., Hewapathirana, S., Kundu, D. J., ... & Pérez, E. The PRIDE database and related tools and resources in 2019: improving support for quantification data. *Nucleic acids research.* 2019;47(D1):D442-D450.

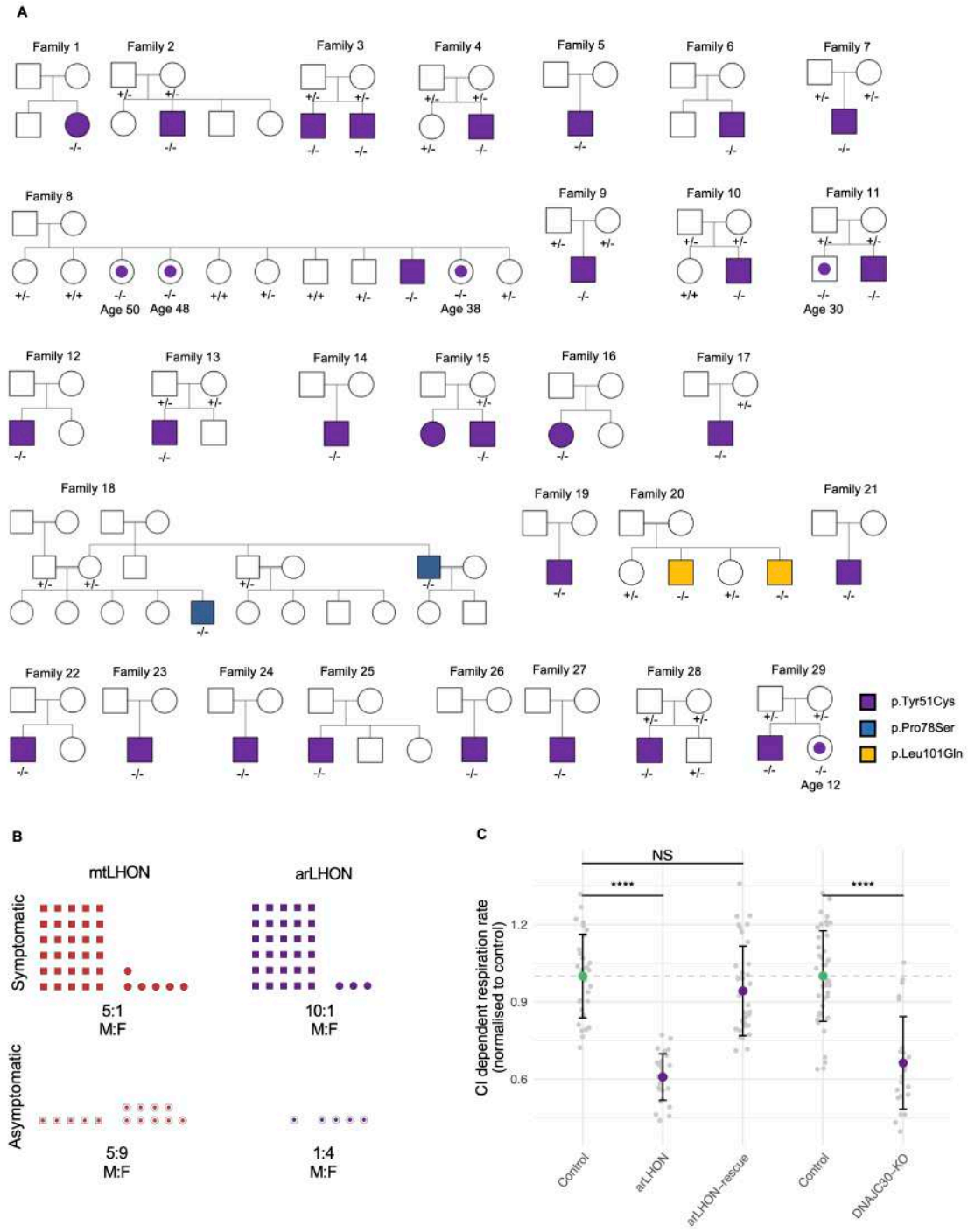
A
Family 1
Family 2
Family 3
Family 4
Family 5
Family 6
Family 7
Family 8
Family 9
Family 10
Family 11
Family 12
Family 13
Family 14
Family 15
Family 16
Family 17
Family 18
Family 19
Family 20
Family 21
Family 22
Family 23
Family 24
Family 25
Family 26
Family 27
Family 28
Family 29
Age 50
Age 48
Age 38
Age 30
Age 12
p.Tyr51Cys
p.Pro78Ser
p.Leu101Gln
B
mtLHON
arLHON
Symptomatic
Asymptomatic
5:1
M:F
10:1
M:F
5:9
M:F
1:4
M:F
C
NS
****
****
CI dependent respiration rate
(normalised to control)
1.2
0.9
0.6
Control
arLHON
arLHON-rescue
Control
DNAJC30-KO

Figure 1. Identification of pathogenic *DNAJC30* mutations in LHON patients in association with a complex I defect.

(A) Pedigrees from 29 families. The genotype is denoted by (-/-) for homozygous variant carriers, (+/-) for heterozygous variant carriers, and (+/+) for carriers of two wild-type alleles. Individuals with a central dot are homozygous carriers (-/-) whom do not express the disease phenotype at their current age, stated beneath. **(B)** Schematic of the gender dependent incomplete penetrance in both maternally inherited LHON (mtLHON) and recessive LHON (arLHON) demonstrating a clear male predominance in symptomatic carriers of disease-causing variants. **(C)** Mitochondrial complex I (CI) dependent respiration rate measurement in control (n=30, technical replicates) and arLHON (n=28, technical replicates) fibroblast cells lines, demonstrating a mild respiratory defect rescued by re-expression of naïve DNAJC30 (arLHON-rescue, n=36, technical replicates). The defect in CI dependent respiration rate is recapitulated in the *DNAJC30*-KO (n=25, technical replicates) in comparison to control (n=43, technical replicates) HEK cell lines. Data are normalized to the respective control cell line and depicted by the mean ± s.d.; two-sided Student's t-test, p values corrected for multiple comparisons to the control (Dunnett's test).

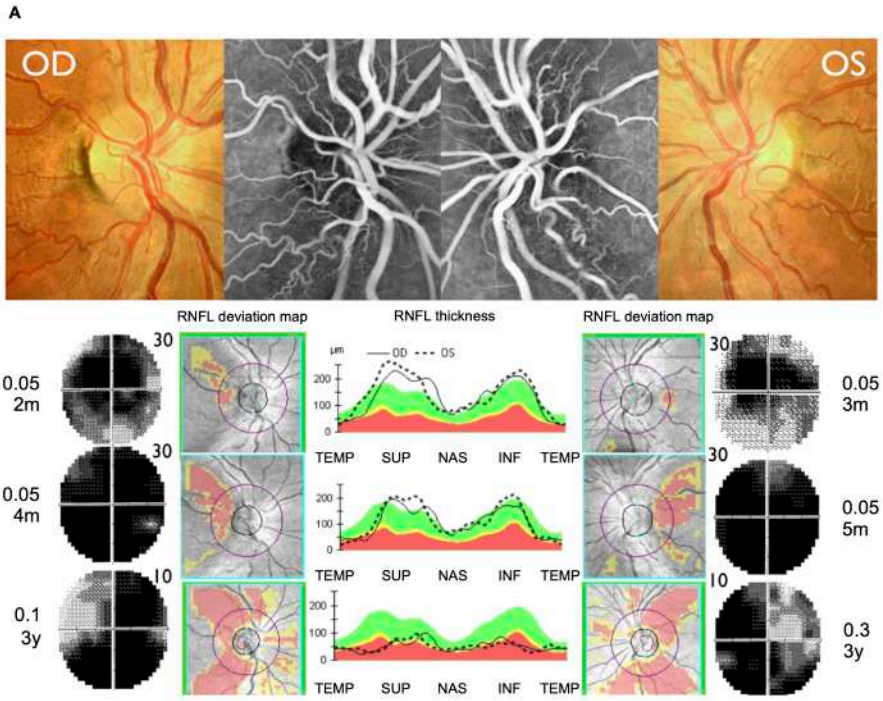
A
OD
OS
RNFL deviation map
RNFL thickness
RNFL deviation map
30
10
0.05
2m
0.05
4m
0.1
3y
0.05
3m
0.05
5m
0.3
3y
µm
OD
OS
200
100
0
TEMP
SUP
NAS
INF
TEMP

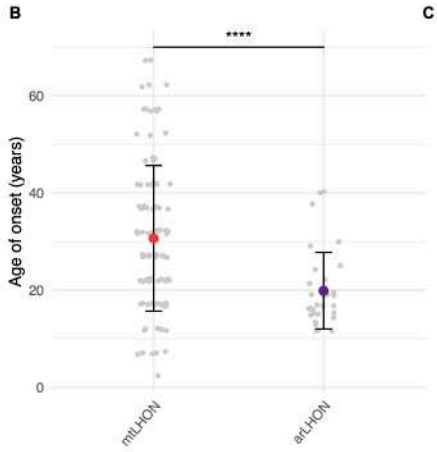
B
****
Age of onset (years)
60
40
20
0
mtLHON
arLHON

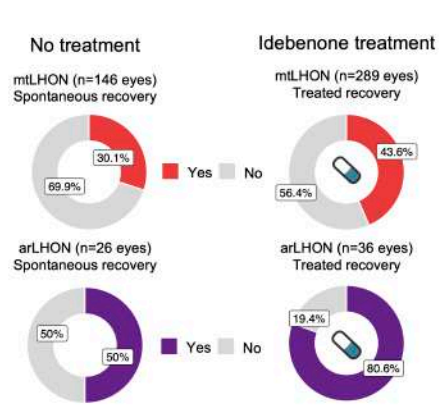
C
No treatment
Idebenone treatment
mtLHON (n=146 eyes)
Spontaneous recovery
30.1%
69.9%
Yes
No
mtLHON (n=289 eyes)
Treated recovery
43.6%
56.4%
arLHON (n=26 eyes)
Spontaneous recovery
50%
50%
Yes
No
arLHON (n=36 eyes)
Treated recovery
19.4%
80.6%

Figure 2. LHON associated with *DNAJC30* mutations presents as a phenocopy of maternally inherited LHON.

(A) The pathognomonic triad of ophthalmological features in mtLHON are recapitulated in arLHON. Presented here is an illustrative example from one arLHON patient. Top panel: Optic nerve head picture and fluorescein angiography in the acute stage of the disease displaying microangiopathy without leakage, fiber swelling, and initial temporal pallor of the optic disc. Bottom panel: The RNFL (retinal nerve fiber layer) thickness analysis and deviation map showing the progressive thinning of fibers from the subacute stage (OD at two months and OS at three months after visual loss) to chronic stage (three years). The 30° Humphrey visual field shows progressive enlargement of the central scotoma in the subacute stage (from two to four months in OD and from three to five months in OS) and fenestration of the scotoma after three years (10° Humphrey visual field) associated with recovery of visual acuity (VA, expressed in decimals units). OD: right eye; OS: left eye; m: months; y: years. **(B)** Age of onset (years) in mtLHON (n=104) (28) and arLHON (n=31) ($p<0.0001$, mean ± s.d; two-sided Student's t-test). **(C)** Spontaneous and idebenone treated rate of clinically significant recovery of visual acuity (VA), defined as improvement in logMAR VA of ≥0.2, in mtLHON (4,5,6) in comparison to arLHON, where treated recovery rates demonstrated to be significantly higher in arLHON (mtLHON 43.6%, arLHON 80.6%, $p<0.001$, Fisher's exact test).

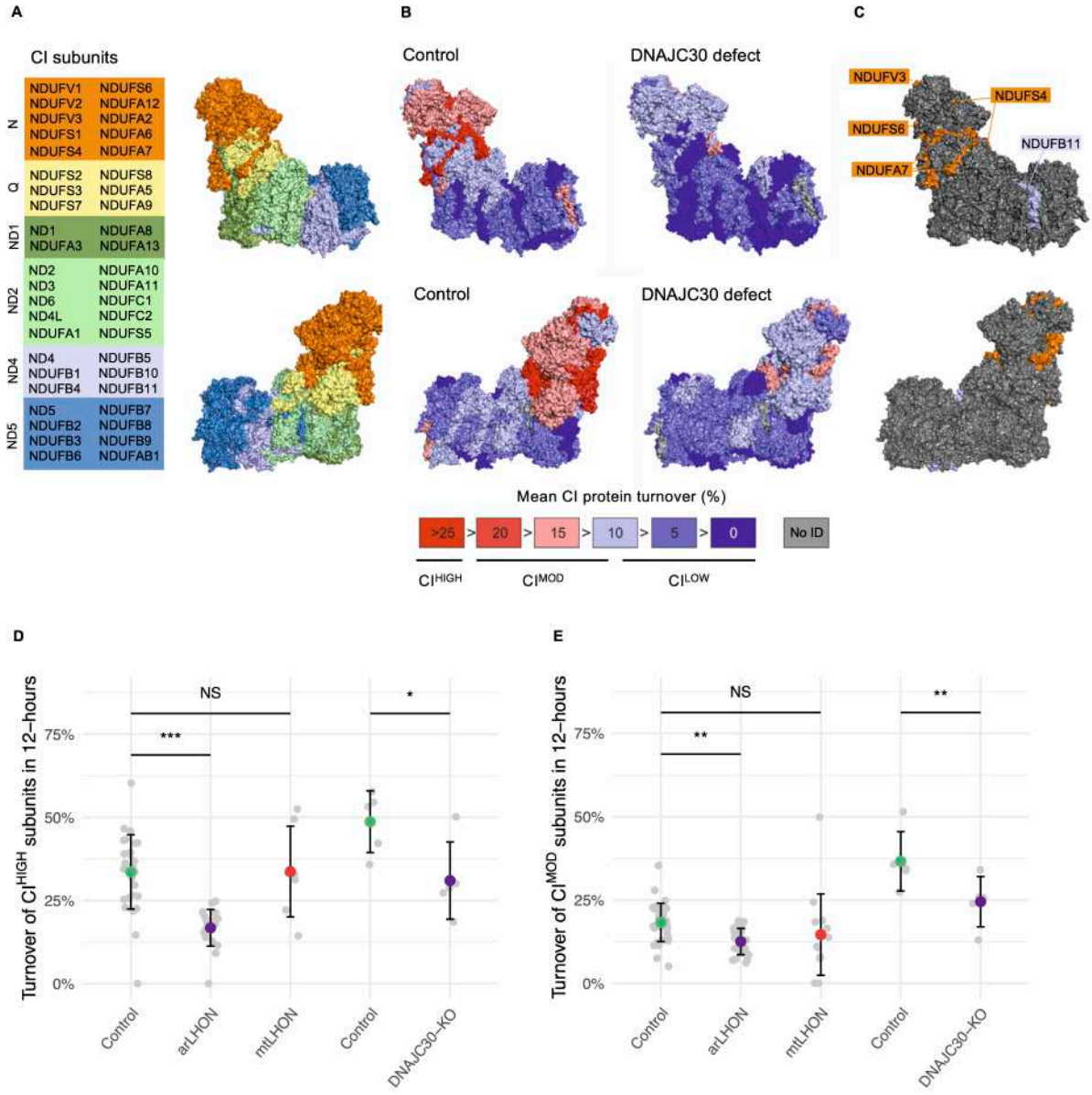
A
CI subunits
N
NDUFV1 NDUFS6
NDUFV2 NDUFA12
NDUFV3 NDUFA2
NDUFS1 NDUFA6
NDUFS4 NDUFA7
Q
NDUFS2 NDUFS8
NDUFS3 NDUFA5
NDUFS7 NDUFA9
ND1
ND1 NDUFA8
NDUFA3 NDUFA13
ND2
ND2 NDUFA10
ND3 NDUFA11
ND6 NDUFC1
ND4L NDUFC2
NDUFA1 NDUFS5
ND4
ND4 NDUFB5
NDUFB1 NDUFB10
NDUFB4 NDUFB11
ND5
ND5 NDUFB7
NDUFB2 NDUFB8
NDUFB3 NDUFB9
NDUFB6 NDUFAB1
B
Control
DNAJC30 defect
Control
DNAJC30 defect
C
NDUFV3
NDUFS4
NDUFS6
NDUFB11
NDUFA7
Mean CI protein turnover (%)
>25 > 20 > 15 > 10 > 5 > 0
No ID
CI^HIGH
CI^MOD
CI^LOW
D
Turnover of CI^HIGH subunits in 12–hours
75%
50%
25%
0%
NS
***
*
Control
arLHON
mtLHON
Control
DNAJC30–KO
E
Turnover of CI^MOD subunits in 12–hours
75%
50%
25%
0%
NS
**
**
Control
arLHON
mtLHON
Control
DNAJC30–KO

Figure 3. *DNAJC30* mutations result in impaired repair of specific subunits of mitochondrial complex I.

(A) The structure of mitochondrial CI (30), depicted by module and respective protein. **(B)** Mitochondrial CI structure colored by the mean degree of subunit turnover by 12-hours in control cell fibroblast lines (n=7) and patient fibroblast cell lines (n=6) depicted as a percentage (%). The mean data are provided in **Table S15** and the individual experiments are depicted in **Table S11-S14**. **(C)** The DNAJC30 interacting partners in CI according to the Bioplex database highlighted on the CI structure. The interaction partners in the N-module (NDUFV3, NDUFS4, NDUFS6, and NDUFA7) account for four of the five CI^{HIGH} subunits, defined as subunits with >25% turnover in 12-hours in the control fibroblast cell lines. **(D)** Turnover measurement of CI^{HIGH} subunits (n=5) and **(E)** CI^{MOD} subunits (n=5) by 12-hours in control (n=7), arLHON (n=6), and mtLHON patient (n=3, m.3460G>A in *MT-ND1*, m.11778G>A in *MT-ND4*, and m.14484T>C in *MT-ND6*) fibroblast cell lines, and control (n=1) and *DNAJC30*-KO (n=1) HEK cell lines. arLHON patients demonstrate a defect in CI^{HIGH} (control mean 33.6% ± 11.2% s.d., patient mean 16.8% ± 5.5% s.d., $p<0.0001$) and CI^{MOD} (control mean 18.3% ± 5.7% s.d., patient mean 12.5%. ± 3.9% s.d., $p<0.001$) subunits. The defective turnover of CI^{HIGH} subunits is shown to be specific to arLHON (CI^{HIGH} subunits, control mean 33.6% ± 11.2% s.d., mtLHON mean 33.7%. ± 13.7% s.d., p 0.98). The *DNAJC30*-KO HEK cell line demonstrates a defect in CI^{HIGH} (control mean 48.7%. ± 8.3% s.d., KO mean 31.0%. ± 11.6% s.d., p 0.013) and CI^{MOD} (control mean 36.6%. ± 8.9% s.d., KO mean 24.5%. ± 7.5% s.d., p 0.002) subunits. Data depicted as the mean ± s.d.; two-sided Student's t-test, p values corrected for multiple comparisons to the control (Dunnett's test). A complete summary of the data is provided in **Table S10** and the experiment is depicted in **Table S10-S15** and **S17**.

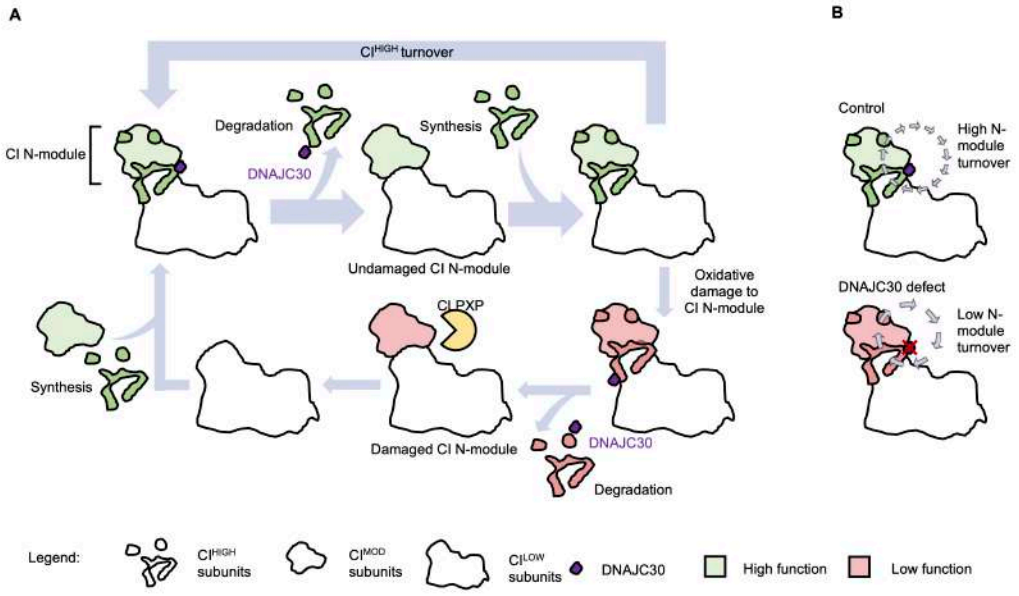
A
B
CI^HIGH turnover
CI N-module
Degradation
DNAJC30
Synthesis
Undamaged CI N-module
Oxidative damage to CI N-module
CLPXP
Synthesis
Damaged CI N-module
DNAJC30
Degradation
Control
High N-module turnover
DNAJC30 defect
Low N-module turnover
Legend:
CI^HIGH subunits
CI^MOD subunits
CI^LOW subunits
DNAJC30
High function
Low function

Figure 4. Schematic representation of the proposed role of DNAJC30 in complex I repair. **(A)** In normal physiological conditions, DNAJC30 interacts with specific CI N-module proteins (CI^{HIGH}) facilitating their disassembly and subsequent degradation. In the setting of highly functional CI, these proteins are newly synthesized and replaced without degradation of further subunits. While, in the case of oxidative damage to the CI N-module, upon disassembly of the CI^{HIGH} subunits by DNAJC30 the protease CLPXP may access and remove the damaged CI^{MOD} subunits (20-21). Along with the CI^{HIGH} subunits, these subunits are subsequently resynthesized and replaced, negating the need for complete degradation and synthesis of CI at high energetic cost. **(B)** Compared to control, in the presence of *DNAJC30* mutations turnover of the N-module subunits is decreased, impairing the CI repair mechanism and leading to the accumulation of lowly functioning CI.

Table 1. Summary of all subjects

Subject ID	Country of origin	Gender	Age of onset (years)	Age of last follow-up (years)	Clinical phenotype	Haplogroup
1	Germany	Female	2	21	Leigh syndrome	K1a3a1
2	Luxemburg	Male	19	25	LHON	H4a1a1a
3-1	Poland	Male	29	32	LHON	J1c+16261
3-2	Poland	Male	17	30	LHON	J1c+16261
4	Romania	Male	16	18	LHON	H
5	Russia	Male	20	-	LHON	H2a2b1
6	Russia	Male	14	16	LHON	J1c3f
7	Ukraine	Male	17	20	LHON	H56
8	Russia	Male	38	39	LHON	T2c1d1a
9	Russia	Male	13	24	LHON	U5b3
10	Russia	Male	13	15	LHON	J1c8a
11	Russia	Male	24	30	LHON	U4a
12	Russia	Male	15	23	LHON	H15a1
13	Russia	Male	19	25	LHON	H15a1
14	Russia	Male	28	30	LHON	H4a1
15-1	Russia	Male	17	28	LHON	H2a
15-2	Russia	Female	25	25	LHON	H2a
16	Russia	Female	40	49	LHON	H6a1a
17	Russia	Male	15	29	LHON	U2e2a1a
18-1	Tunisia	Male	16	25	LHON	H7c
18-2	Tunisia	Male	Unclear	48	LHON	H7c
19	Canada	Male	15	17	LHON	-
20-1	Turkey	Male	19	20	LHON	G2a2a
20-2	Turkey	Male	12	31	LHON	G2a2a
21	Russia	Male	21	22	LHON	HV9b
22	Russia	Male	22	23	LHON	I1b
23	Russia	Male	19	19	LHON	U4a

24	Russia	Male	16	17	LHON	-
25	Russia	Male	16	22	LHON	-
26	Russia	Male	40	40	LHON	J1c2f
27	Russia	Male	12	19	LHON	-
28	Ukraine	Male	12	12	LHON	-
29	Ukraine	Male	15	15	LHON	-

Table 2. Ophthalmological clinical features of all arLHON subjects

Subject ID	Time to involvement of second eye (weeks)	Time to nadir (weeks, OD/OS)	Visual acuity at nadir (logMAR, OD/OS)*	Visual acuity at last visit (logMAR, OD/OS)*	CRR of VA (OD/OS)	Complete recovery of VA (OD/OS)	Visual field defect	Idebenone treatment
2	12	40/32	(1.60/1.40)	(1.68/1.68)	(N/N)	(N/N)	Central scotoma	Yes
3-1	12	2/8	(1.40/2.00)	(1.40/2.00)	(N/N)	(N/N)	Central scotoma	Yes
3-2	Bilateral onset	12-14/12-14	(2.00/2.00)	(0.30/0.40)	(Y/Y)	(N/N)	Central scotoma	No
4	1	52/52	(1.68/1.68)	(1.10/1.10)	(Y/Y)	(N/N)	Central scotoma	Yes
5	Bilateral onset	-	(2.00/2.00)	(1.30/0.50)	(Y/Y)	(N/N)	-	Yes
6	4	8/4	(2.00/1.00)	(1.00/0.00)	(Y/Y)	(N/Y)	-	Yes
7	4	8/8	(2.30/2.30)	(1.00/0.50)	(Y/Y)	(N/N)	-	Yes
8	Bilateral onset	12/12	(1.00/1.00)	(0.10/0.10)	(Y/Y)	(N/N)	Central scotoma	Yes
9	Bilateral onset	12/12	(1.40/1.50)	(0.54/0.00)	(Y/Y)	(N/Y)	Central scotoma	No
10	8	16/16	(1.10/1.10)	(0.00/0.00)	(Y/Y)	(Y/Y)	Central scotoma	Yes
11	Bilateral onset	2/2	(2.00/2.00)	(1.92/1.51)	(Y/Y)	(N/N)	Central scotoma	Yes
12	Bilateral onset	8/8	(1.40/1.40)	(0.30/0.90)	(Y/Y)	(N/N)	Central scotoma	Yes
13	16	4/4	(1.40/1.40)	(0.70/0.70)	(Y/Y)	(N/N)	Central scotoma	Yes
14	Bilateral onset	16/16	(1.40/1.40)	(0.00/0.10)	(Y/Y)	(Y/N)	Central scotoma	Yes
15-1	Bilateral onset	8/8	(1.90/1.20)	(0.18/0.18)	(Y/Y)	(N/N)	Central scotoma	Yes
15-2	Bilateral onset	-	(1.51/1.40)	(1.51/1.40)	(Y/Y)	(N/N)	Central scotoma	No
16	2	4/4	(1.68/1.68)	(1.30/1.60)	(Y/N)	(N/N)	Central scotoma	No
17	Bilateral onset	4/4	(1.10/1.10)	(1.31/1.11)	(N/N)	(N/N)	Central scotoma	Yes
18-1	Bilateral onset	0/0	(1.68/1.30)	(0.10/0.10)	(Y/Y)	(N/N)	Central scotoma	No
18-2	-	-	-	-	(N/N)	(N/N)	Central/peripheral	No
19	24	4/4	(0.60/1.30)	(0.70/1.30)	(N/N)	(N/N)	Central scotoma	No

20-1	Bilateral onset	52/52	(1.00/1.00)	(1.00/1.00)	(N/N)	(N/N)	Central scotoma	No
20-2	-	-	-	-	(Y/Y)	(N/N)	-	No
21	24	12/9	(1.70/1.70)	(0.87/0.28)	(Y/Y)	(N/N)	Central scotoma	Yes
22	1	12/11	(2.00/1.40)	(0.59/0.41)	(Y/Y)	(N/N)	Central scotoma	Yes
23	1	14/15	(1.20/1.35)	(0.98/1.03)	(Y/Y)	(N/N)	Central scotoma	Yes
24	24	24/1	-	(0.27/0.02)	-	-	Central scotoma	No
25	Bilateral onset	14/14	(2.00/2.00)	(0.00/0.00)	(Y/Y)	(Y/Y)	Central scotoma	No
26	Bilateral onset	-	-	(1.00/1.00)	(N/N)	(N/N)	Central scotoma	No
27	48	-	(-/1.11)	(0.18/0.00)	(Y/Y)	(N/Y)	Central scotoma (OD only)	No
28	12	-	(0.40/0.40)	(0.10/0.00)	(Y/Y)	(N/N)	Central scotoma	Yes
29	Bilateral onset	-	-	-	(N/N)	(N/N)	Central scotoma	No

Off-chart visual acuity is defined as logMAR 1.68 and counting fingers/hand motion/light perception is defined as logMAR values of 2.0/2.3/2.6; LogMAR (Logarithm of the Minimum Angle of Resolution); OD (right eye); OS (left eye); CRR (clinically relevant recovery); VA (visual acuity); Data unavailable is denoted by (-).